Power Management and Control Strategies for Off-Grid Hybrid Power Systems with Renewable Energies and Storage

Belkacem Belabbas [1, 2], Tayeb Allaoui [1], Mohamed Tadjine [2], Mouloud Denai [3]

[1] University of Tiaret, L2GEGI Laboratory, Tiaret, Algeria

[2] School of Polytechnic National, LCP Laboratory, Algiers, Algeria

[3] School of Engineering and Technology, University of Hertfordshire, Hatfield, UK

Abstract

This paper presents a simulation study of standalone hybrid Distributed Generation Systems (DGS) with Battery Energy Storage System (BESS). The DGS consists of Photovoltaic (PV) panels as Renewable Power Source (RPS), a Diesel Generator (DG) for power buck-up and a BESS to accommodate the surplus of energy, which may be employed in times of poor PV generation. While off-grid DGS represent an efficient and cost-effective energy supply solution particularly to rural and remote areas, fluctuations in voltage and frequency due to load variations, weather conditions (temperature, irradiation) and transmission line short-circuits are major challenges. The paper suggests a hierarchical Power Management (PM) and controller structure to improve the reliability and efficiency of the hybrid DGS. The first layer of the overall control scheme includes a Fuzzy Logic Controller (FLC) to adjust the voltage and frequency at the Point of Common Coupling (PCC) and a Clamping Bridge Circuit (CBC) which regulates the DC bus voltage. A maximum power point tracking (MPPT) controller based on FLC is designed to extract the optimum power from the PV. The second control layer coordinates among PV, DG and BESS to ensure reliable and efficient power supply to the load. MATLAB Simulink is used to implement the overall model of the off-grid DGS and to test the performance of the proposed control scheme which is evaluated in a series of simulations scenarios. The results demonstrated the good performance of the proposed control scheme and effective coordination between the DGS for all the simulation scenarios considered.

Keywords: Standalone, Distributed generation; Photovoltaic; Diesel generator; Energy storage; Fuzzy logic control.

Nomenclature

V_{DG_abc}	Voltage of the DG
I_{DG_abc}	Current of the DG
V_{Load_abc}	Voltage of the Load
I_{Load_abc}	Current of the Load
V_{f_abc}	Voltages of inverter
I_{f_abc}	Filtered currents of inverter
P_e	Power balance between generation and consumption
P_{PV}	Photovoltaic system output power
P_{batt}	Battery power
P_{Load}	Load power
P_{DG}	Diesel generator power
V_{batt}	Voltage of the Battery
I_{batt}	Current of the Battery
I_{batt}^{*}	Reference current of the battery
L_1	Inductor of DC-DC boost converter
L_2	Inductor of bidirectional DC-DC converter.
C_B	Capacitor of DC-DC boost converter
L_f	Inductive filter
C	Capacitor of inverter
V_{dc}	DC-link voltage
V_{dc}^{*}	Reference of DC-link voltage
I_{dc}	DC-link current
R_1, C_1	Effests created by mass transport
R_2, C_2	Effests created by the charge transfer
R	Conducting resistance
V_{OC}	Open-circuit voltage
I	Charge or discharge current
C_r	Rated capacity
M	Multiple or fraction of C_r
t	Time.
P, Q	Active and reactive powers
P^{*}, Q^{*}	References of active and reactive powers
V_{L_d}, V_{L_q}	Direct and quadrature of PCC voltage
I_{L_d}, I_{L_q}	Direct and quadrature of load current
ω	Pulse
ω^{*}	Reference of pulse
E	Maximum voltage
E^{*}	Reference of maximum voltage
n	Droop of active power coefficient
m	Droop of reactive power coefficient

1. INTRODUCTION

Standalone Distributed Generation Systems (DGS) consisting of small-scale power generation and BESS to supply electricity close to the point of consumption are a viable solution for the future development of electric power infrastructure in remote localities where the connection to the main grid is difficult or not affordable. Recently Hybrid Power Systems (HPS) integrating a combination of PV, Wind Power (WP) and Distributed Generation (DG) sources with BESS have been successfully deployed to power telecom base positions and for the electrification of remote areas in several countries across the world as reported in [1]–[6]. As reported in [6], the selection of the appropriate configuration of hybrid installation for a given site depends on several factors including the load power requirement, site geography, the topographical features and climate of the region in terms of availability of RES, cost of BESS and delivery, seasonal energy requirements, etc.

Several HPS arrangements have been described in the literature such as PV/DG power systems without BESS, PV/BESS/DG, PV/WP/BESS, PV/WP/BESS/DG, PV/WP/DG without BESS, PV/WP, PV/WP/DG/Micro-hydro electric turbine and PV/WP/Fuel cell [7].

Standalone HPS have been studied by few authors [1]–[6], [8], [9]. In [1], the authors proposed an approach to enhance the operation of a stand-alone PV/DG/BESS, however, the voltages and frequency profiles at the Point of Common Coupling (PCC) are not discussed. In [2], a PV/DG/BESS is proposed for an isolated area, but the overall control system and power quality issues are not studied. In [3], a PV/DG system without BESS for off-grid operation has been presented. Again, the complete control system of the voltages and frequency is not discussed. The authors in [4] proposed the control of an autonomous HPS for a single-phase system. Moreover, BESS and dump load which makes the system unreliable was not considered. A Fuzzy Logic Control (FLC) of the frequency in a PV/DG/BESS has been proposed in [5], [6], [8]. In [5], a control method of the frequency for the PV/DG hybrid system with BESS is presented. However, the control system of the DC voltage is not discussed. In [6], a study on the feasibility of PV/DG hybrid plants in Algeria is presented, but the complete control system control is not discussed. In [9], a PV/DG hybrid system is proposed to supply power to a building where the battery is directly connected to the DC bus, but the control of the battery power flow through a bidirectional converter is not discussed. In [10], the dynamic behavior of a standalone HPS is studied. However, the controls of the converter, PV and BESS are not presented.

Another important element that plays a major role in off-grid DGS is the BESS. Nowadays, lithium-ion (Li-ion) batteries are commonly employed to stock the surplus of energy derived from RPS and release it at a later stage. It has higher power density and voltage range as compared to other BESS [11].

The hybrid DGS considered in this study consists of PV panels as RPS, a DG for power back-up, and a BESS. The DG is employed as a secondary power source when both PV and BESS are not able to satisfy the power required by the load.

For a reliable and efficient operation of the proposed off-grid HPS, it is necessary to develop a Power Management (PM) algorithm to ensure energy balance between demand, production and storage [12]–[14]. The PM should be able to handle all possible scenarios: load variation, changing weather and Short Circuit Fault (SCF). It must respond quickly to the energy needs of the load and maintain stability of DC voltage. The PM also provides protection of the overall HPS.

Voltage variations at the PCC, fluctuation of the DC bus voltage and harmonic generation are the major power quality issues that occur in off-grid HPS. The two first are mainly due to sudden changes in the load power demand or the occurrence of a SCF in the line. But, the harmonics generation is the result of power electronic converters switching.

To address the problem of unbalanced DC voltage, a controller based on a Clamping Bridge Circuit (CBC) is used to set the voltage of DC bus when there is a variation in the load power and/or following the occurrence of a SCF. The use of BESS in HPS also contributes to stability of DC voltage.

To control the voltage at the PCC, a classical Proportional-Integral (PI) controller is commonly employed, owing to its simple structure and ease of implementation. However, such a design requires a linearized model of the system, which is difficult to obtain and may not give satisfactory performance under challenging operating conditions such as system's parameter variations. In this paper, a FLC is applied to maintain the voltage and frequency at the PCC. Fuzzy logic is a powerful mathematical concept for modeling imprecision, vagueness and uncertainties which characterise real-world systems. This concept has its foundation from the theory of Fuzzy Sets (FSs) introduced in 1965 by Zadeh and which assigns a degree of membership to the elements of a set in contrast to the classical bivalent logic. As mentioned in [15], FLC has good features like robustness against parameter variations and improved control accuracy.

The principal objective of this contribution is to propose a control scheme for an off-grid HPS in order to improve the reliability and power quality and enhance the robustness of HPS against SCFs in the lines connecting the sources or at the PCC. The control scheme includes (1) voltage and frequency regulation of the voltage source inverter at the PCC,

(2) clamping-bridge circuit to stabilize the DC bus voltage, (3) a PM algorithm to coordinate between PV/DG/BESS under different scenarios and provide the protection of the HPS.

The paper is organised as follows: Section 2 describes the proposed off-grid HPS including a presentation of the PV system and its MPPT control strategy, the Li-ion battery model with the buck-boost DC-DC converter and its control and the sizing of the DG. The control strategies of HPS are presented in Section 3. The simulation results and conclusion are presented in Section 4 and 5 respectively.

2. MODELING OF THE OFF-GRID HPS

The proposed off-grid HPS (PV/DG/BESS) is presented in Fig. 1. The DC bus and AC bus are interfaced via a DC-AC inverter whose output is passed through an inductive filter. During night-time, when PV power is not available, the DG and BESS must supply the required power to the load and regulate the frequency and voltage of the isolated HPS in PCC. Therefore, a buck-boost DC-DC converter is connected between the DC bus and BESS and the DG is coupled directly to the AC load.

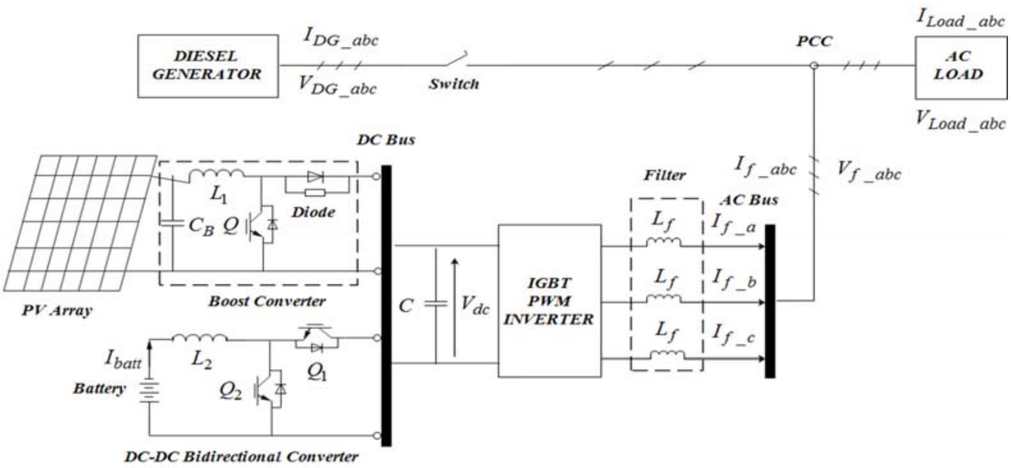

Fig. 1 Proposed standalone HPS.

2.1 PV Modeling and MPPT Controller Design

A. PV array model

A basic equivalent circuit model of a PV cell is depicted in Fig. 2

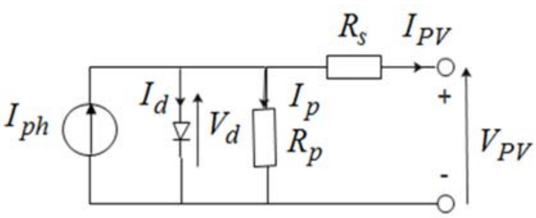

Fig. 2 PV cell circuit model.

Where I_{ph} is Light-Generated Current (LGC), I_d is the current of the diode, I_p is the current flowing through the parallel resistor R_p, I_{PV} is the net current of the PV cell, V_{PV} is cell voltage, V_d is the diode voltage, R_p and R_s are the parallel and series resistances of the cell respectively.

Applying Kirchhoff's law, the current I_{PV} of the cell is:

$$I_{PV} = I_{ph} - I_d - I_p \tag{1}$$

$$I_p = \frac{V_{PV} + R_s I_{PV}}{R_p} \tag{2}$$

The current I_d is given by:

$$I_d = I_0 \left[e^{\frac{V_{PV}+R_s I_{PV}}{aV_t}} - 1 \right] \tag{3}$$

The equation relating the current and voltage in the circuit is written as:

$$I_{PV} = I_{ph} - I_0 \left[e^{\frac{V_{PV}+R_s I_{PV}}{aV_t}} - 1 \right] - \frac{V_{PV} + R_s I_{PV}}{R_p} \tag{4}$$

$$V_t = \frac{N_s K T}{q} \tag{5}$$

Where I_0 is the diode saturation current, a is the diode ideality factor, V_t is the thermal voltage, N_s represents the number of cells connected in series, K denotes the Boltzmann's constant, T is the actual temperature and q is the charge of the electron.

The LGC of an elementary PV cell is difficult to determine because it is influenced by both resistors. Data sheets only provide the nominal short -circuit current ($I_{sc,n}$), which is the maximum current which can be generated from the PV cell. A commonly used assumption in PV models is $I_{sc} \approx I_{PV}$ since in practical devices R_p is high and R_s is low. With this assumption, the LGC can be expressed as:

$$I_{ph} = (I_{sc} + K_I \Delta_T) \frac{G}{G_n} \tag{6}$$

Where I_{sc} is short -circuit current, $\Delta_T = T - T_n$ (T_n is nominal temperature), G and G_n are the irradiation and nominal irradiation on the device surface respectively.

The current I_0 may be expressed as:

$$I_0 = \frac{I_{sc,n} + K_I \Delta_T}{\left(\frac{V_{oc,n} + K_V \Delta_T}{aV_t} \right) - 1} \tag{7}$$

Where $V_{oc,n}[V]$ is the nominal open-circuit voltage, K_V and K_I are the voltage and current coefficients.

B. Design of the MPPT

Fig. 3 depicts the structure of the boost circuit and MPPT controller for the PV.

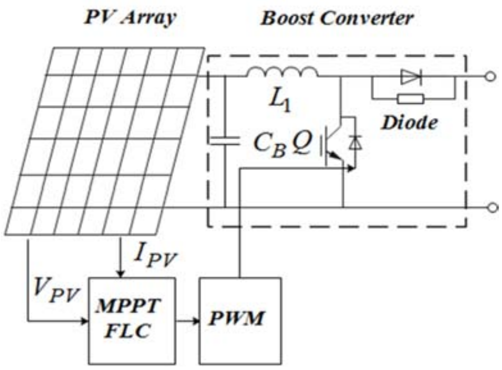

Fig. 3 Boost circuit and MPPT for the PV.

Several MPPT algorithms have been applied in the literature to extract the optimal power from PV. The Perturb & Observe [16]–[18] and Incremental Conductance [19]–[21] are the most commonly used in MPPT algorithms.

In this paper, the MPPT algorithm is based on FLC which provides a simple design methodology and does not require information about the exact model of the system. Similar FLC-based MPPT controllers have been applied in [16], [21]–[27].

The basic scheme of a FLC is presented in Fig. 4. The inputs are the error E and error change dE, and the output is the duty cycle variation D which is practicaced to the DC-DC converter to control the output voltage of the PV.

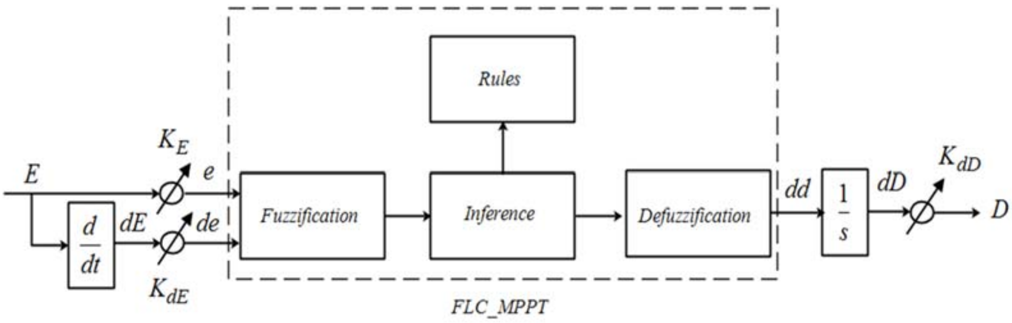

Fig. 4 Bloc diagram of a FLC_MPPT.

The instantaneous power of the PV generator is given by:

$$P_{PV}(k) = V_{PV}(k).I_{PV}(k) \tag{8}$$

In the MPPT algorithm, the ratio of dP/dV is instantly calculated, so the first input (E) of FLC can be determined as follows:

$$E = \frac{dP}{dV}(k) = \frac{P_{PV}(k) - P_{PV}(k-1)}{V_{PV}(k) - V_{PV}(k-1)} \tag{9}$$

The second input of the FLC is defined as the deviation of the error dE:

$$dE = \Delta\left(\frac{dP}{dV}(k)\right) = \frac{dP_{PV}}{dV_{PV}}(k) - \frac{dP_{PV}}{dV_{PV}}(k-1) \tag{10}$$

$$dE = E(k) - E(k-1) \tag{11}$$

The duty cycle change dD is obtained using the next discrete-time difference equation:

$$dD(k) = dd(k) - dd(k-1) \tag{12}$$

The e, de and D are normalized as follows:

$$\begin{cases} e = K_E E \\ de = K_{dE} dE \\ D = K_{dD} dD \end{cases} \tag{13}$$

Where K_E, K_{dE} and K_{dD} are scaling gains selected to achieve the required response characteristics [29].

The universe of discourse of e, de and D are divided into three FSs with triangular and trapezoidal Membership Functions (MFs) labelled NS (Negative Small), Z (Zero) and NB (Negative Big) as shown in Fig. 5. The fuzzy rules used to represent the controller output are summarized in Table 1.

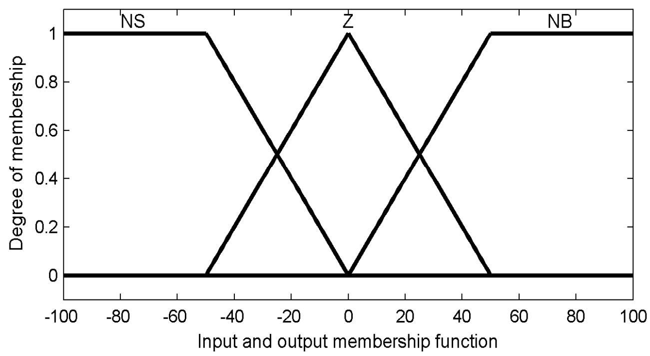

Fig. 5 MFs of the MPPT_FLC.

Table 1 Rules of FLC.

dE \ E	**NS**	**Z**	**NB**
NS	NS	NS	Z
Z	NS	Z	NB
NB	Z	NB	NB

The defuzzification is based on the centre of gravity method.

$$dd = \frac{\sum_{i=1}^{n}[\mu(dd_i)dd_i]}{\sum_{i=1}^{n}[\mu(dd_i)]} \tag{14}$$

2.2 BESS modeling and control

Energy Storage (ES) systems are classified into two categories depending on the range of power (high or small) required for the integration of RPS. High-ES systems such as SMES (Magnetic Energy Storage) are more popular for RES applications in particular the PV systems. However, the major difficulty of SMES is their high cost for implementation [30]. Small-ES systems, such as flywheels, fuel cells and batteries, are more often used in medium and low power PV applications. Different types of BESS technologies are currently available in the HPS [11]. In this paper, a Lithium-ion (Li-ion) battery model is used [31]-[37]. Li-ion batteries can achieve highest energy density and the high efficiencies of ES up to 100 % when compared to other types of batteries [11]. However, the principal drawbacks of Li-ion batteries are expensive cost and reduction in lifetime. Therefore, it is recommended not to over-discharge the battery below 20% of its State Of Charge (SOC) to extend its lifetime [35], [38].

A. Li-ion battery model

Fig. 6 presents the equivalent circuit of a Li-ion battery [38], [39]. The model includes a SOC controlled voltage source and its equivalent impedance which is also a function of SOC. There is a straightforward analogy between this model and real batteries because all the coefficients and parameters can be obtained experimentally. In this paper, the effects of temperature, age or self-discharging for this battery are not taken into account.

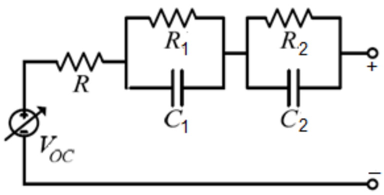

Fig. 6 Equivalent circuit model of a Li-ion battery.

The BESS is characterized by its rate of charge or discharge defined as follows:

$$I = MC_r t \tag{15}$$

In theory, the BESS would provide its rated capacity in a well-estimated time when operating at the nominal current of discharge. In practice, the discharge of the BESS is less than the estimated time owing to inefficiencies in the discharge cycle. BESS charging management algorithms are discussed in more details in [40], [41].

B. BESS charge and discharge management

The goal is to control the BESS current to accomplish the required power. BESS will operate in charging or discharging modes depending of the energy requirements. The additional role of the BESS is to maintain the DC voltage at the desired level in response to diverse operating conditions of the HPS. The overall control system of the BESS is depicted in Fig. 7.

When BESS is charging (discharging), switch Q_2 (Q_1) is on and the converter operates in boost (buck) mode. Furtheremore, if the DC voltage drops below the reference, switch Q_1 is on otherwise switch Q_2 is on. The response of HPS to transient variations is characterised by an inherent time constant. In such cases, capacitors along the DC-link can act as a virtual inertia to supply the lack or absorb the surplus of energy. The control of DC link voltage has been discused in [1], [4], [10], [19], [36], [39], [42].

If the losses in the converters and battery are neglected, the balance of power at the capacitor of the DC link for the integrated PV system with BESS is governed by:

$$V_{dc}I_{dc} = P_{PV} + P_{batt} - P_{Load} \tag{16}$$

$$V_{dc}I_{dc} = CV_{dc}\frac{dV_{dc}}{dt} = P_{PV} + P_{batt} - P_{Load} \tag{17}$$

If the PV power is equal to that of the load, the battery will supply the required power to the capacitor in order to regulate the DC voltage.

The transfer function between P_{batt} and V_{dc} is given by:

$$\frac{V_{dc}(s)}{P_{batt}(s)} = \frac{1}{sCV_{dc}} \tag{18}$$

Where s represents the Laplace variable.

With:

$$P_{batt} = V_{batt}I_{batt} \tag{19}$$

Equation (18) becomes

$$\frac{V_{dc}(s)}{I_{batt}(s)} = \frac{V_{batt}}{sCV_{dc}} \tag{20}$$

The BESS reference current I_{batt}^{*} can be obtained from a DC bus voltage feedback loop based on a PI controller as follows:

$$I_{batt}^{*} = \left(K_{vP} + \frac{K_{vI}}{s}\right)(V_{dc}^{*} - V_{dc}) \tag{21}$$

Finally, a hysteresis controller is applied to control the DC-DC converter switches Q_1 or Q_2 and regulate the BESS current I_{batt}.

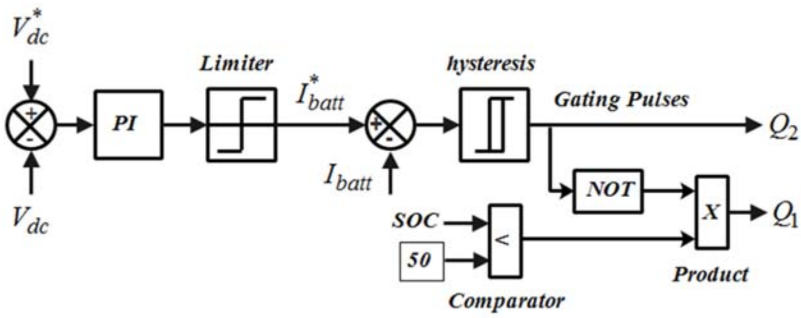

Fig. 7 Overall arrangement of the battery converter controller.

Where K_{vP} and K_{vI} are the proportional and integral gains of the PI controller.

Instability and unbalance of output DC voltage are considered as the main problem in converters. This can be overcome by inserting a Clamping-Bridge Circuit (CBC) in parallel with the capacitor as shown in Fig. 8. The CBC consists of an electronic switch T in series with a resistance r_p.

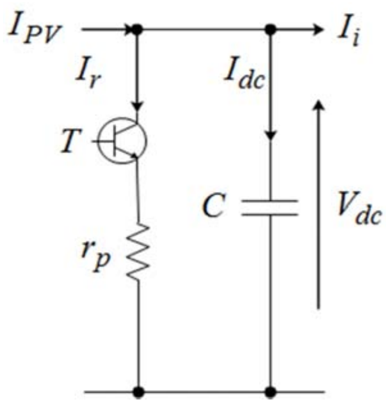

Fig. 8 CBC configuration.

With reference to Fig. 8.

$$V_{dc} = \frac{1}{C}\int (I_{PV} - I_r - I_i)dt \tag{22}$$

Where I_r is current flowing over r_p and I_i is the input current to the inverter.

$$I_r = T\frac{V_{dc}}{r_p} \tag{23}$$

The CBC compares the error between the measured DC voltage and its reference. If the error is different from 0, the extra energy will be dissipated through the resistance, this control algorithm is given as follows:

$$\begin{cases} V_{dc}^{*} - V_{dc} = \epsilon \qquad V_{dc}^{*} = 600\,V \\ \text{if } \epsilon > 0 \quad \text{then} \quad T = 1 \implies I_r = \dfrac{V_{dc}}{r_p} \\ \qquad\qquad \text{else} \quad T = 0 \implies I_r = 0 \end{cases} \tag{24}$$

2.3 Modeling of the Diesel Generator

The DG normally operates at nominal power and any surplus of energy can be employed to charge the BESS. In general, the DG is usually designed to operate between 80 % and 100 % of its rated power [43], while running together with the BESS or other RES. The output voltage of the DG is regulated to the AC bus voltage, therefore in most situations DGs are coupled in parallel to achieve the current requirements [1], [3]–[5], [8], [44]. The energy (E_{DG}) generated by DG is given by:

$$E_{DG} = P_{DG}\eta_{DG}t \tag{25}$$

Where η_{DG} denotes the efficiency of the DG.

3 CONTROL STRATEGIES OF HPS

The proposed control scheme for the off-grid HPS consists of two layers:

- A local control layer which includes:
  a) A FLC-based inverter voltage and frequency regulator at the PCC.
  b) A DC bus voltage controller to compensate for imbalance caused by load variations and transmission line short-circuits.
- A supervisory control layer which includes the PM and coordination between PV, DG and BESS.

3.1 Inverter voltage and frequency control

The aim is to design a robust control strategy to keep the voltage and frequency of the inverter at their desired values irrespective of the disturbances acting on the system such as fluctuations in solar irradiance, load variations and TPSC fault in the transmission line.

In the HPS, the sources are usually located far apart and measurement quantities are not easily accessible, therefore it is necessary to develop a control algorithm for the inverter that uses only the local variables that can be measured easily.

Droop is generally used control scheme in power systems to control the voltage and frequency of the inverter [45]–[48]. Using droop control, the active and reactive powers distribution by the inverters is automatically attained by controlling the voltage amplitude and frequency of the inverter. As presented in Fig. 9, it contains of an inner loop for voltage control and an outer loop to control the power. A PI regulator is commonly employed to adjust the voltage for this strategy. However, other control techniques, such as, FLC, sliding mode control, and predictive control have been proposed in [5], [8], [19]. In this study, a FLC is proposed.

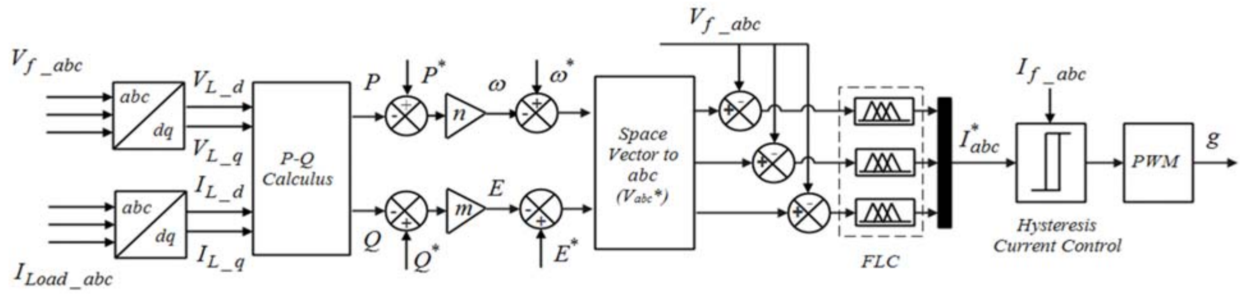

Fig. 9 Inverter control system based on droop and FLC controls.

The real (P) and reactive (Q) powers are calculated from the PCC voltage (V_{f_abc}) and the load current (I_{Load_abc}) which are expressed in the stationary frame by their d-q components (V_{L_d}, V_{L_q}) and (I_{L_d}, I_{L_q}) respectively. Therefore, P and Q powers are defined as follows:

$$\begin{cases} P = \frac{3}{2}\left(V_{L\_d}.I_{L\_d} + V_{L\_q}.I_{L\_q}\right) \\ Q = \frac{3}{2}\left(V_{L\_q}.I_{L\_d} - V_{L\_d}.I_{L\_q}\right) \end{cases} \tag{26}$$

The calculated powers are compared with their references values (P* and Q*) and the differences are fed into the droop controller defined as follows:

$$\begin{cases} \omega = n(P - P^*) \\ E = m(Q - Q^*) \end{cases} \tag{27}$$

The FLC based inner voltage control loop forces the inverter output voltage to track the desired reference E*.

The outputs of this voltage compensator together with the inner filter inductor currents are then fed into an inner current compensator to produce the PWM control signals. Fig. 10 shows the bloc diagram of the voltage controller. The voltage error (e_V) and the derivative of the voltage errors (de_V) are used as inputs to the FLC. Its output is integrated in order to determine the reference current I^*_{abc}.

Where K_1, K_2 and K_3 are adaptive gains.

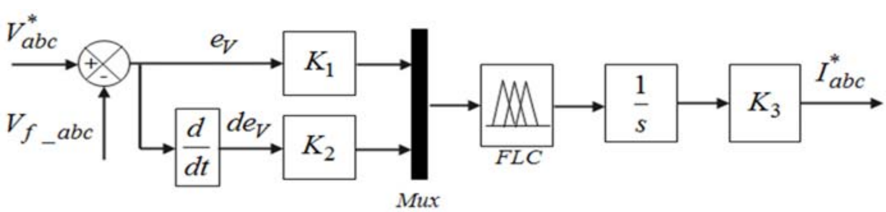

Fig. 10 FLC structure of voltage controller.

The input and output variables of the FLC are defined by seven triangular and trapezoidal MFs which is illustrated in Fig. 11. The method of min–max inference is employed for generate the rules of the FLC which are summarized in Table 2. The defuzzification is based on the centre of gravity method.

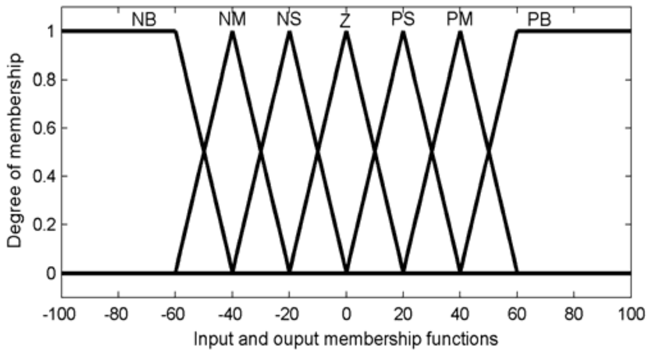

Fig. 11 MFs of the FLC voltage controller.

Table 2 Rule base of the FLC voltage controller.

Output		de_V						
		NB	**NM**	**NS**	**Z**	**PS**	**PM**	**PB**
e_V	**NB**	NB	NB	NB	NB	NM	NS	Z
	NM	NB	NB	NB	NM	NS	Z	PS
	NS	NB	NB	NM	NS	Z	PS	PM
	Z	NB	NM	NS	Z	PS	PM	PB
	PS	NM	NS	Z	PS	PM	PB	PB
	PM	NS	Z	PS	PM	PB	PB	PB
	PB	Z	PS	PM	PB	PB	PB	PB

Where the MF labels are defined as: PB (Positive Big), PM (Positive Medium), PS (Positive Small), Z (Zero), NB (Negative Big), NM (Negative Medium) and NS (Negative Small).

3.2 Supervisory Control System

Fig. 12 presents a flowchart for the Supervisory Control System (SCS) for the off-grid HPS. The role of the SCS is to balance the power generated from HPS (PV / DG / BESS) with the power demanded by the load.

Initially, after ensuring that the PV generates its optimum power, the SCS compares the load power with the power generated from PV system based on this equation:

$$P_e = P_{PV} - P_{Load} \tag{28}$$

- Firstly, it should be stressed that the DG operates when the load exceeds 14 kW to compensate for the difference in energy between the PV and power demand.

- If P_e is positive and if the BESS connected to PV is completely charged, the PV provides the necessary energy to the load, if not the energy surplus between the PV and load power is stored in the BESS.
- On the other hand, if P_e is negative, the DG is used to supply energy to the load. Next, the complete power generated from DG and PV is compared with the load power. If P_e is positive and the BESS is completely charged, then the power of PV is used by the load. If not, the BESS is charged from the power difference among the PV, DG and the load. In this step, P_e is negative, this means that the total power generated by both DG and PV is less than the power demanded by the load, then if the BESS is discharged and SOC is close to 20 %, for this condition the BESS works in the Charge-Sustaining Mode (CSM) and the PM strategy stops discharging the BESS. So, the load consumes the power provided by the PV and DG. If not, the BESS provides the energy to the load to support the power delivered by the PV and DG.

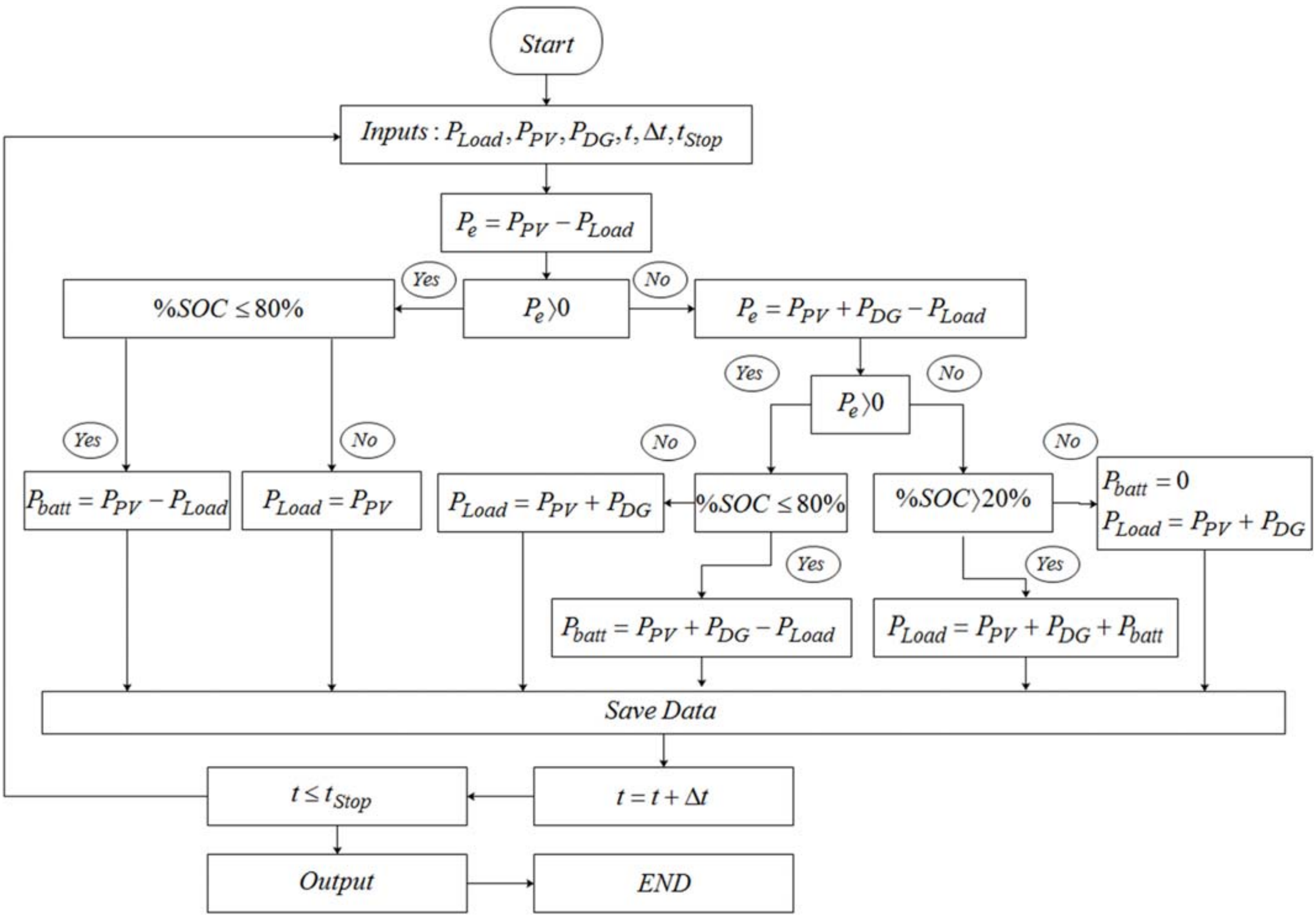

Fig. 12 Flowchart of the SCS.

4 SIMULATION RESULTS AND DISCUSSION

MATLAB/SIMULINK is employed to implement the model of the proposed off-grid HPS and test the performance of the controllers. The overall model and control scheme have been simulated for three diverse scenarios which described in the following sub-sections. Parameter values used in the overall model are showed in the Appendix.

A. Step change in insolation

In this first scenario, the system of Fig. 1 is simulated with a variable solar irradiance. As illustrated in Fig. 13, the irradiance is initially set at 1000 W/m^2 and the stepped down to 800 W/m^2 and 600 W/m^2 at $t = 0.5\ s$ and $t = 0.8\ s$ respectively.

Fig. 14 shows the active power of the PV, DG and the load demand which is assumed to be constant and equal to 13.7 kW. The BESS power, current, voltage and SOC are presented in Fig. 15 (a, b, c and d) respectively.

It is assumed that, initially, the PV generated power is greater than the power required by the load and the BESS is partially charged.

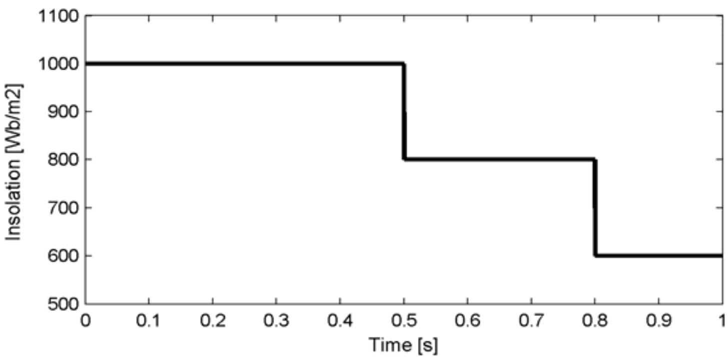

Fig. 13 Simulated changes in the solar irradiance.

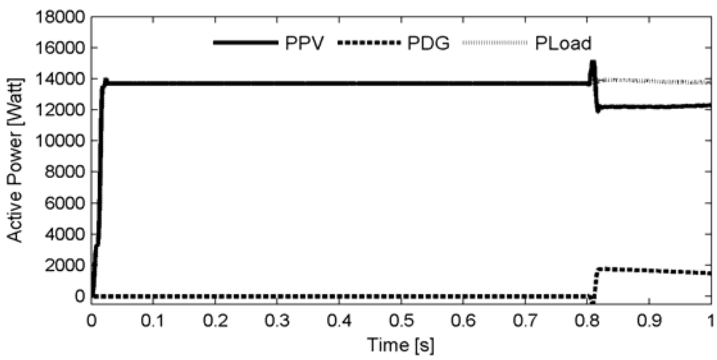

Fig. 14 Active power of the PV (solid), DG (dotted) and the active required (dashed).

At $t = 0.8\ s$ the PV generation is lower than the load demand. The DG should respond quickly and provide the difference between the power demanded by the load and that available from the PV. In this case, the BESS delivers the energy to the load to support the power delivered by PV and DG. These results demonstrate the effectiveness of PM.

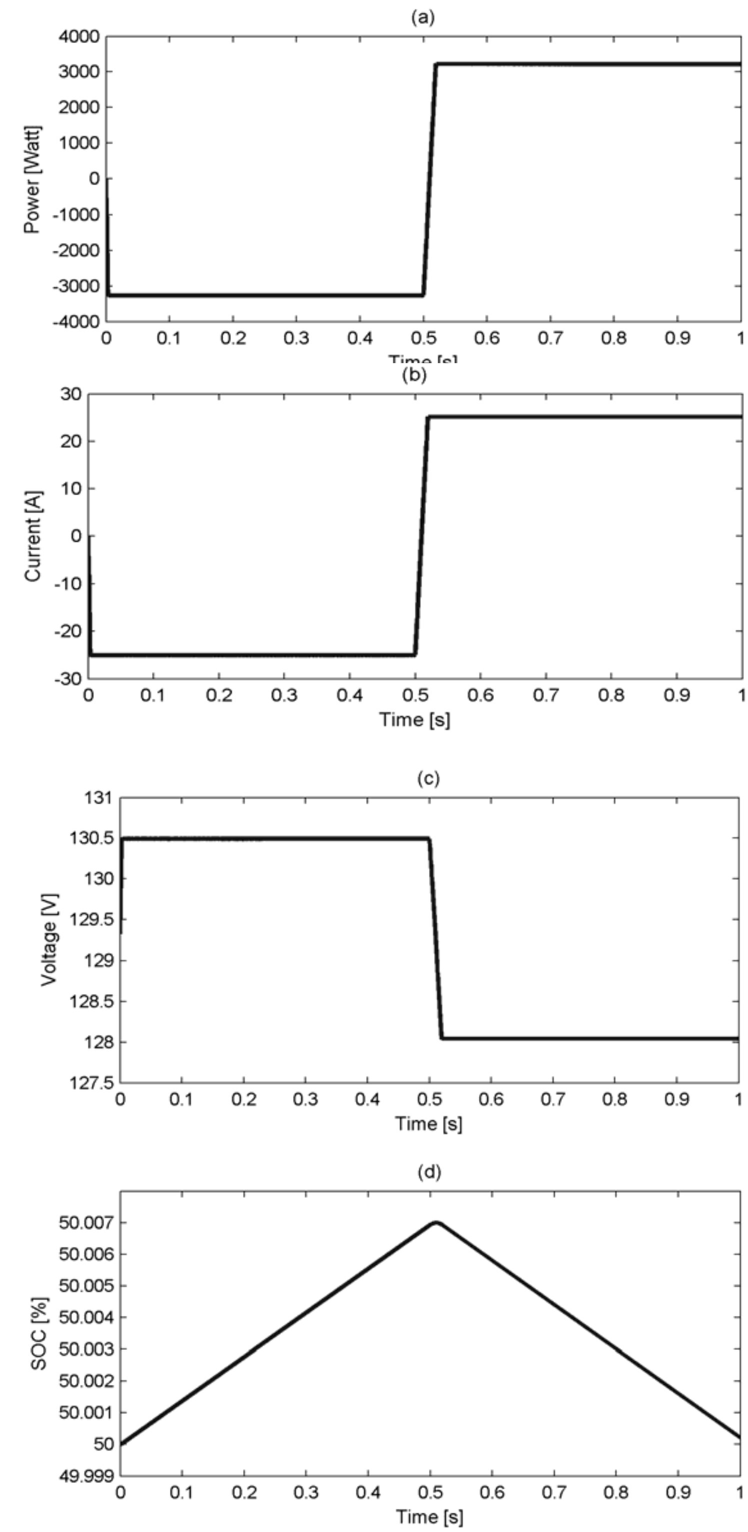

Fig. 15 Battery response (a) Power (b) Current (c) Voltage (d) SOC.

As can be seen from Fig. 16, the DC voltage is successfully maintained at 600 V after the insolation is varied at $t = 0.8\ s$ which proves the effectiveness of the CBC used. These results are reflected by the stability of the midpoint.

The load current shown in Fig. 17 has a fast dynamic response, a stable and sinusoidal waveform.

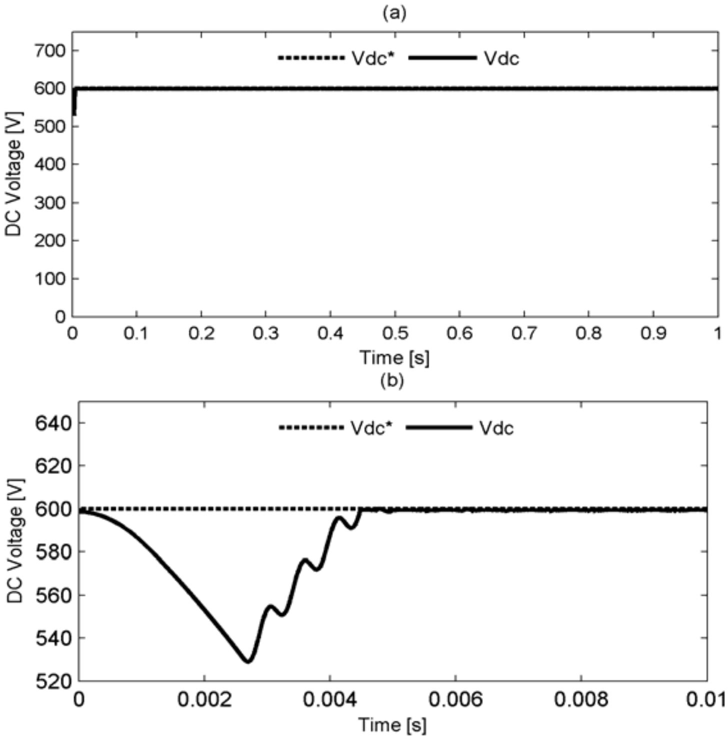

Fig. 16 (a) DC voltage and (b) Zoom of (a).

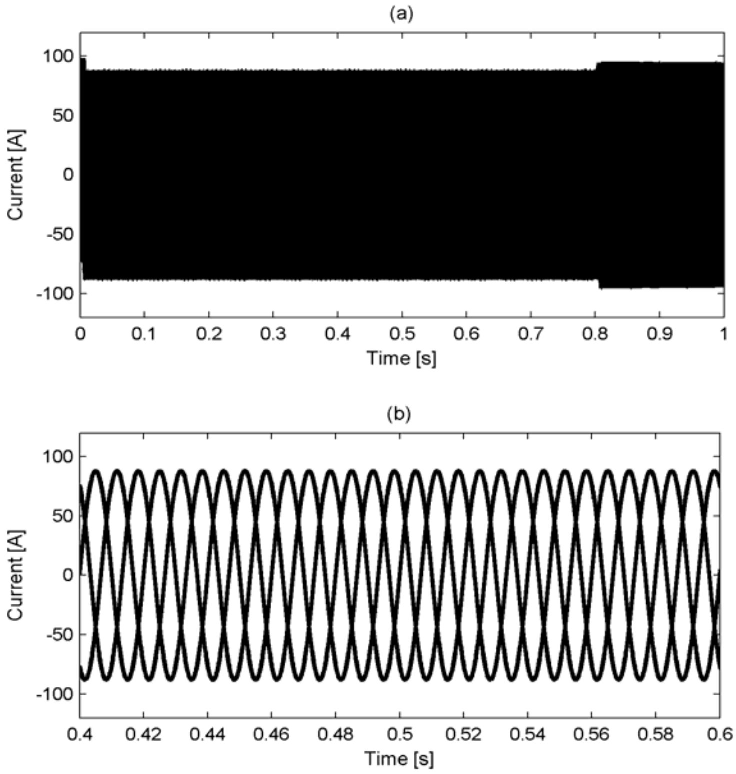

Fig. 17 (a) Load current waveforms and (b) Zoom of (a).

Figs. 18, 19 and 20 show the voltage at the PCC, the corresponding RMS and frequency respectively. From Fig. 18, it can be observed that the voltage waveform remains stable and sinusoidal throughout this simulation. A successful integration of RES in an off-grid HPS requires effective control of the voltage and frequency at the PCC.

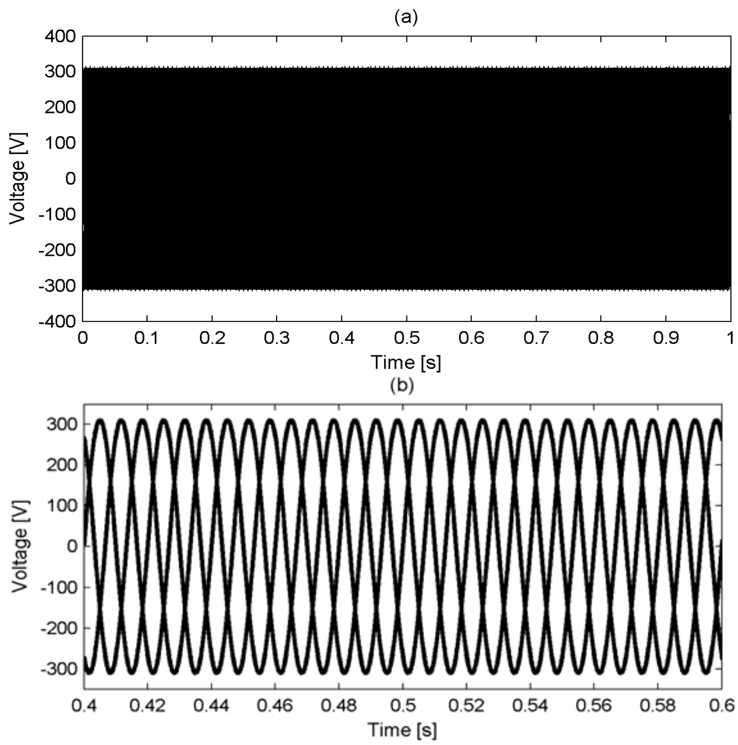

Fig. 18 (a) Voltage at the PCC and (b) Zoom of (a).

To demonstrate the effectiveness of the FLC, a comparison with a PI controller for the control the inverter output voltage is presented. From Fig. 19 it can be observed that the proposed FLC has a better performance and provides a faster transient response than the classical PI controller. Fig. 20 shows some minor fluctuations in the supply frequency, which demonstrates the effectiveness of the control used.

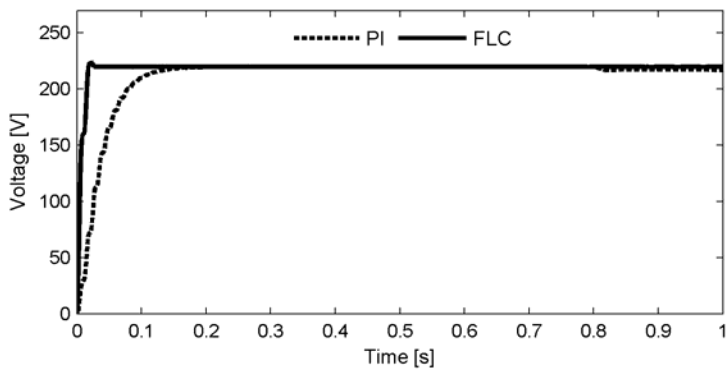

Fig. 19 Voltage RMS at the PCC.

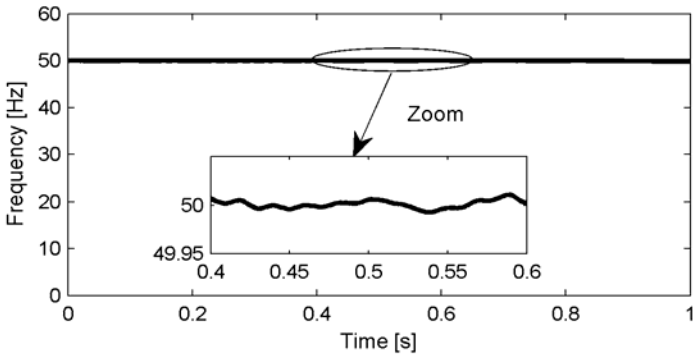

Fig. 20 Frequency.

B. Step change in the load

This scenario is assumed to simulate the system of Fig. 1, for a period with a constant insolation of 1000 W/m^2 and variable load. The load is set to 9 kW initially. At $t = 0.5\ s$ it is suddenly changed to 18 kW and then decreased to 13.7 kW again at $t = 0.8\ s$. The results of this scenario are shown in Figs. 21 to 27.

Fig. 21 shows the power distribution (load, PV and DG). The BESS power, current, voltage and SOC are shown in Fig. 22 (a, b, c and d) respectively.

Initially, between t = 0 s and t = 0.5 s, the load is varied from 0 kW to 9 kW. The PV can simultaneously supply the power to the load and charges the BESS. Then, the load is increased from 9 kW to 18 kW between t = 0.5 s and 0.7 s. As a result, the PV power increases to meet the sudden increase in the load and the DG regulates the instantaneous output voltage to satisfy the new power demand.

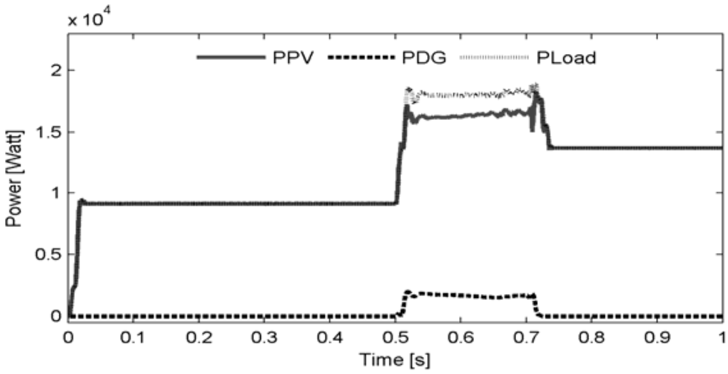

Fig. 21 Active power of the PV (solid), DG (dotted) and the power required (dashed).

Finally, between t = 0.7 s and t = 1 s, the load is varied from 18 kW to 13.7 kW. The BESS also supplies energy to the load to ensure stability between the generated power by the PV / DG and the load demand. In this study, as mentioned earlier, the BESS has two essential roles in the HPS. The first is to supply energy to the load to ensure stability between demand and generation while the second is to ensure the stability of the voltage against DC bus voltage drop. From these results, it can be concluded the PM algorithm is able to achieve good control and balance between the power required by the load and HPS generation under the simulated operating conditions.

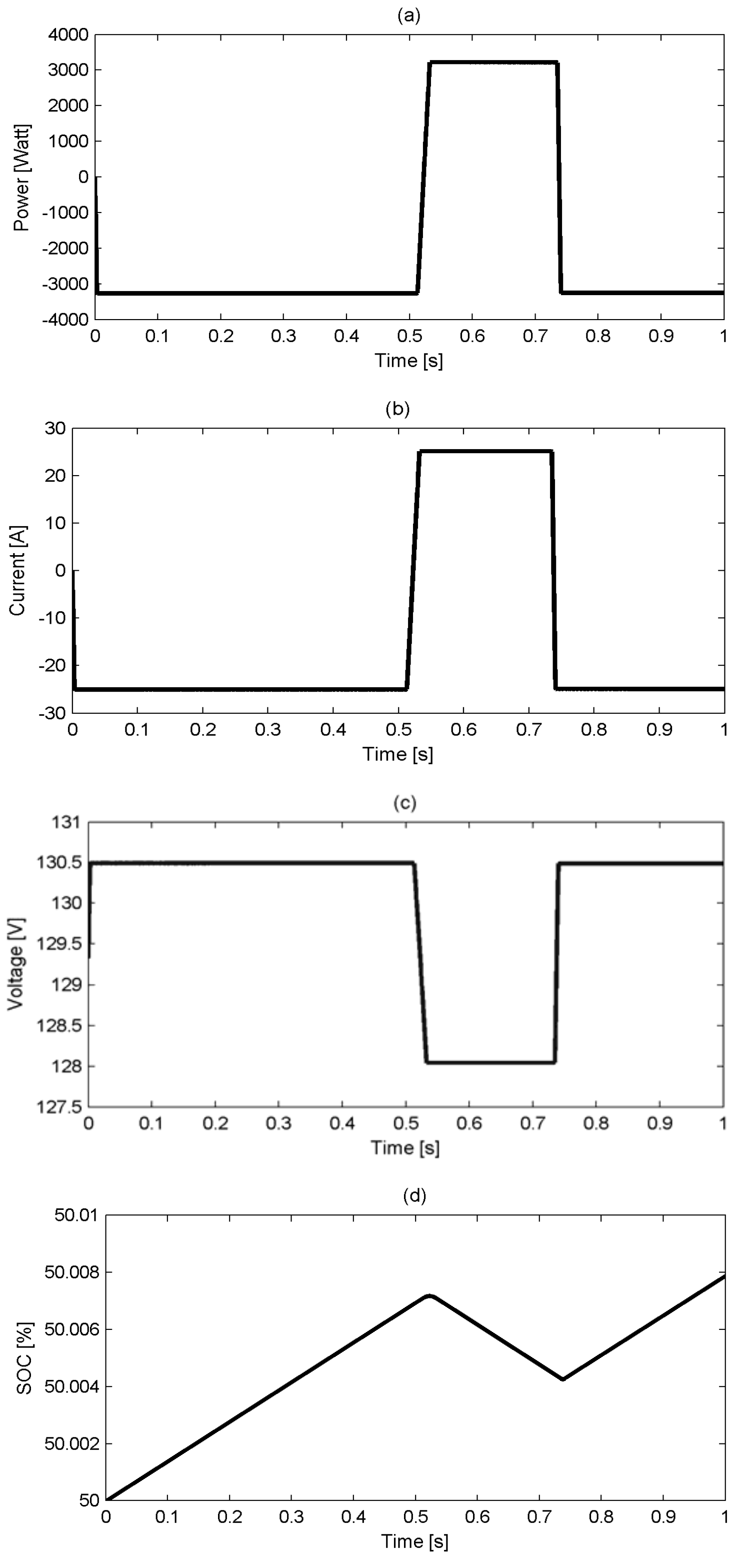

Fig. 22 System performance for Battery (a) Power (b) Current (c) Voltage (d) SOC.

Fig. 23 shows the RMS of the load current, DG current and PV current which are seen to follow the simulated load variations. The direction of the currents at the PCC adopted in these simulations is based the following equation:

$$I_{Load} = I_{PV} + I_{DG} \tag{29}$$

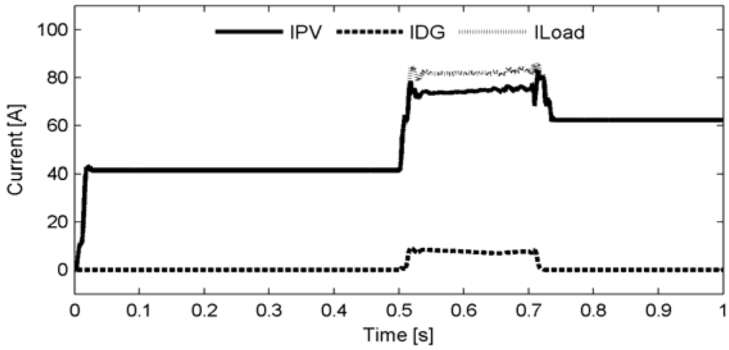

Fig. 23 Current of the PV (solid), DG (dotted) and the current required (dashed).

Figs. 24 and 25 show the three-phase currents of the load and the THD (Total Harmonic Distortion) respectively. From Fig. 24, it can be observed that the current is sinusoidal and its amplitude changes with the load. Furthermore, the THD of the load current is 0.02 % when the PV supplies power to the load. However, when the DG provides energy, the THD is seen to increase to 5.9%.

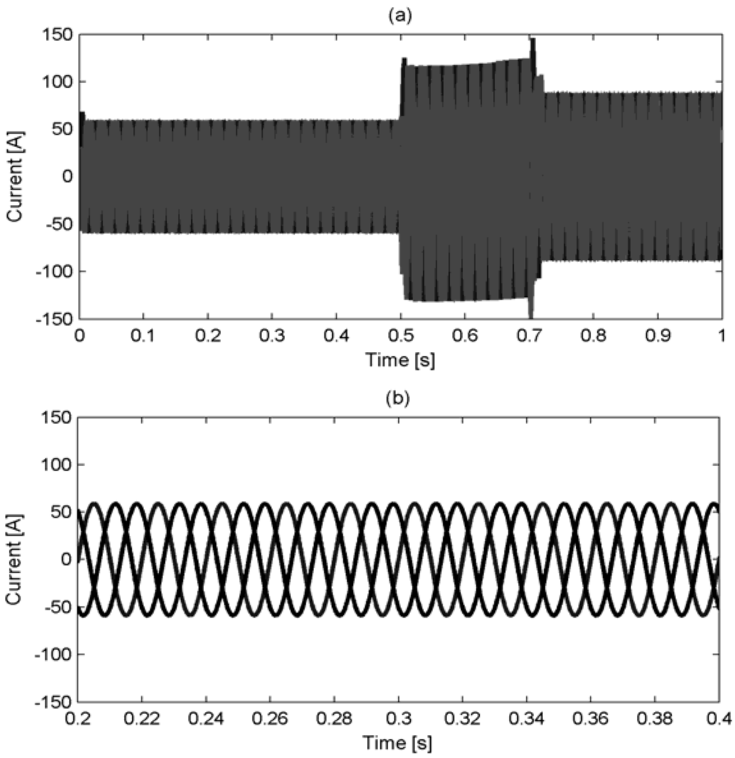

Fig. 24 (a) Load Current waveforms and (b) Zoom of (a).

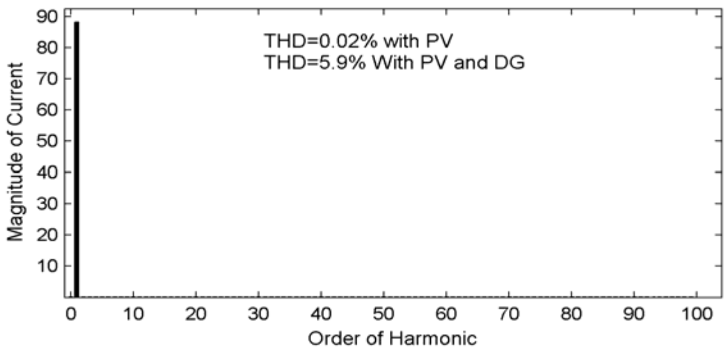

Fig. 25 THD of the current.

To demonstrate the benefits and superior performance provided by the FLC controller against the classical PI controller, a comparative study between PI and FLC is presented for the regulation of the voltage at the PCC for the HPS under variation in the load. Fig. 26 shows the response of RMS voltage at the PCC with PI and FLC. These results show an improved transient response with FLC as compared to PI when a load change is applied.

Fig. 27 shows that the measured DC voltage is successfully regulated at the reference value of 600 V, this results show the effectiveness of the proposed CBC.

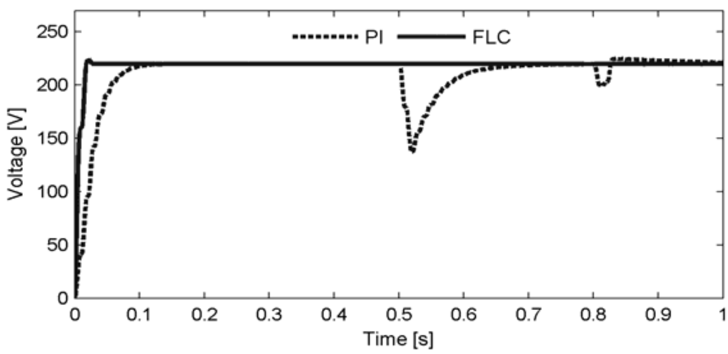

Fig. 26 RMS of the voltage at PCC with FLC (solid) and PI (dashed).

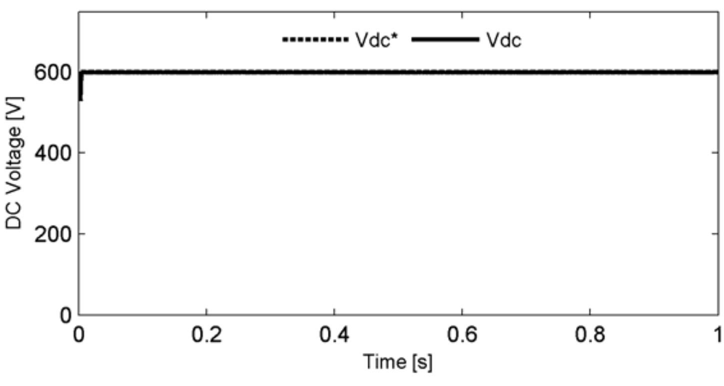

Fig. 27 DC voltage.

In A and B scenarios, the load demand and insolation are varied separately. However, other scenarios can be considered where both load demand and insolation are changed simultaneously since the power management of the HPS is designed to handle any unbalance between load demand and generation.

C. *Three-phase short circuit in the line*

This scenario is simulated with a constant insolation of 1000 W/m^2 and a constant load of 9 kW. The simulated fault is a Three-Phase Short-Circuit (TPSC) on the line and is applied at the PCC at $t = 0.3\ s$ and cleared 10 ms later.

Fig. 28 shows the PV and DG output powers and the load demand. Clearly, the PM algorithm was able to balance the between the power required by the load and HPS generation. At $t\ =\ 0.3\ s$, when the TPSC is applied at the PPC, the system exhibits a transient power unbalance. After the TPSC is cleared, the HPS responds rapidly to provide the power demanded by the load.

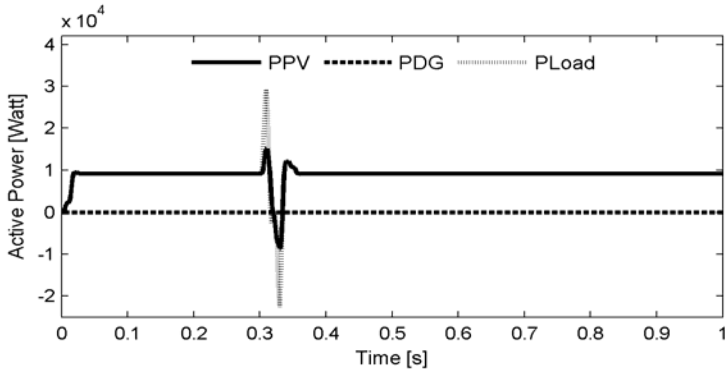

Fig. 28 Active power of the PV (solid), DG (dotted) and the active power required (dashed).

Fig. 29 shows the response of the voltage under this TPSC fault condition. With the FLC, the voltage has a rapid dynamic response and has a superior performance as compared to the PI. Also, it can be noted that at the onset of the TPSC, the voltage becomes almost zero in the case of the PI controller.

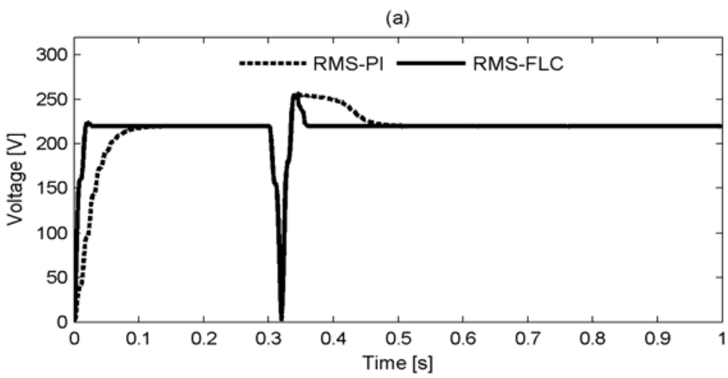

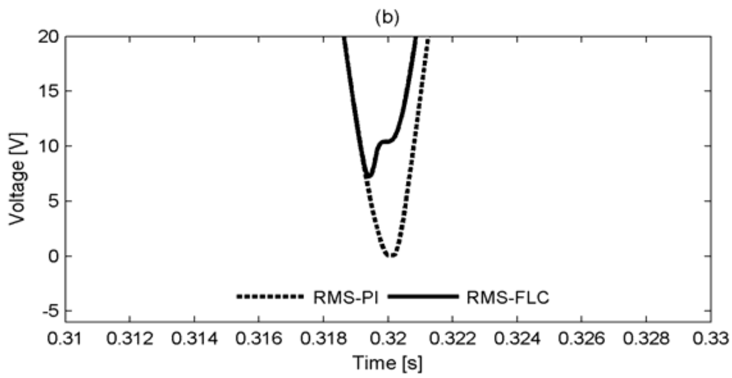

Fig. 29 (a) RMS of the voltage at PCC and (b) Zoom of (a).

The DC link voltage DC is maintained at its reference of 600 V with a short transient following the application of the TPSC as shown in Fig. 30. Furthermore, the robust FLC provides a faster DC link voltage response than the classical PI controller.

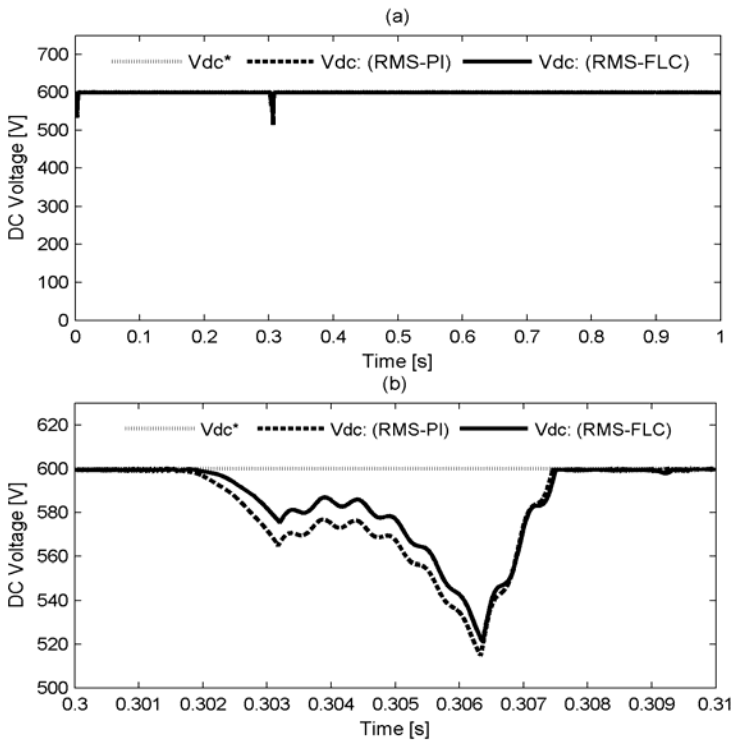

Fig. 30 (a) DC voltage with FLC (solid), PI (dotted), reference (dashed) and (b) Zoom of (a).

Table 3 summarises the comparative results of the FLC and PI controller with respect to the difference scenarios considered in these simulation studies.

Table 3 FLC and PI comparison for the all scenarios studied.

Scenario \ Performance		Average	Good	Excelent
Scenario 1	FLC			✓

	PI		✓	
Scenario 2	FLC			✓
	PI	✓		
Scenario 3	FLC			✓
	PI	✓		

5 CONCLUSIONS

The paper focused on the design and evaluation of a hierachical power management and control scheme for an off-grid HPS consisting of a PV, a DG and a BESS for energy storage.

In this study, two control strategies have been proposed to enhance the performance of the system including the regulation of the voltage and frequency at the PCC using FLC techniques and the design of a CBC to stabilise the DC bus voltage of HPS.

The proposed control scheme has been evaluated in a series of simulations scenarios including load variation, changing solar irradiance and TPSC fault in the transmission line. A comparative simulation study among the proposed FLC and PI controller for the regulation of the voltage is presented and the results demonstrate a superior performance of the FLC. Furthermore, a CBC was proposed to enhance the stability of the DC voltage. The results also demonstrated the effectiveness of the PM algorithm to coordinate between HPS in the different scenarios considered and to provide the protection in HPS.

Acknowledgements:

This work has been supported by Electrical Engineering and L2GEGI laboratory at the Tiaret University, Algeria in collaboration with Polytechnic national school, Algiers, Algeria.

Appendix

Table 4 Parameters of the PV cell (Model KC200GT).

P_{PV}	W	200.143
$V_{oc,n}$	V	32.9
$I_{sc,n}$	A	8.21
$I_{0,n}$	A	$9.825.10^{-8}$
R_p	Ω	415.405
R_s	Ω	0.221

K_V	V/K	-0.123
K_I	A/K	0.0032
a	-	1.3
N_s	-	54
K	J/K	$1.381.10^{-23}$
q	C	$1.602.10^{-19}$

Table 5 DC/DC boost converter parameters.

L_1	µH	11
C_B	mF	1

Table 6 Lithium-ion battery parameters.

V_{batt}	V	120
I_{batt}	A	21.7391
C_r	Ah	50
R	Ω	0.0745
R_1	Ω	0.067
C_1	F	702.72
R_2	Ω	0.0498
C_2	F	$4.47.10^{3}$
V_{OC}	V	3.79

Table 7 DG parameters

$P_{DG,n}$	KW	100
U_{DG}	V	400
Frequency f_{DG}	Hz	50
Friction factor	-	0
Pole pairs	-	2

Table 8 Bidirectional DC/DC converter parameters.

L_2	µH	75

Table 9 Inverter parameters

Snubber resistance	kΩ	5
Snubber capacitor	F	Inf
Internal resistance	mΩ	1
Sampling period T_s	µS	1
Frequency f	Hz	50
V_{dc}	V	600
C	µF	2200

Table 10 Inductive filter value.

L_f	mH	1

Table 11 Controller parameters.

K_{vP}	217
K_{vI}	1
K_{VP}	0.01
K_{VI}	10
n	10^{-3}
m	10^{-4}

REFERENCES

1. Malla, S. G., Bhende, C. N.: Enhanced operation of stand-alone “Photovoltaic-Diesel Generator-Battery” system. Electr. Power Syst. Res. 107, 250–257 (2014)
2. Wies, R. W., Johnson, R., Agrawal, A. N., Chubb, T. J.: Simulink model for economic analysis and environmental impacts of a PV with diesel-battery system for remote villages. Power Syst. IEEE Trans. 20(2), 692–700 (2005).
3. Yamegueu, D., Azoumah, Y., Py, X., Zongo, N.: Experimental study of electricity generation by Solar PV/diesel hybrid systems without battery storage for off-grid areas. Renew. Energy. **36**(6), 1780–1787 (2011)
4. Rashed, M., Elmitwally, A., Kaddah, S.: New control approach for a PV-diesel autonomous power system. Electr. Power Syst. Res. **78(6)**, 949–956 (2008)
5. Datta, M., Senjyu, T., Yona, A., Funabashi, T., Kim, C.-H.: A Frequency-Control Approach by Photovoltaic Generator in a PV–Diesel Hybrid Power System. Energy Convers. IEEE Trans. **26**(2), 559–571 (2011)
6. Khelif, A., Talha, A., Belhamel, M., Arab, A. H.: Feasibility study of hybrid Diesel–PV power plants in the southern of Algeria: Case study on AFRA power plant. Int. J. Electr. Power Energy Syst. **43**(1), 546–553 (2012)
7. Patra, S., Ankur, Narayana, M., Mohanty, S. R., Kishor, N.: Power Quality Improvement in Grid-connected Photovoltaic–Fuel Cell Based Hybrid System Using Robust Maximum Power Point Tracking Controller. Electr. Power Compon. Syst. 1–16 (2015)
8. Datta, M., Senjyu, T., Yona, A., Funabashi, T.: A fuzzy based method for leveling output power fluctuations of photovoltaic-diesel hybrid power system. Renew. Energy. **36**(6), 1693–1703 (2011)
9. Khatib, T., Mohamed, A., Sopian, K., Mahmoud, M.: Optimal sizing of building integrated hybrid PV/diesel generator system for zero load rejection for Malaysia. Energy Build. **43**(12), 3430–3435 (2011)
10. Kalantar, M.: Dynamic behavior of a stand-alone hybrid power generation system of wind turbine, microturbine, solar array and battery storage. Appl. Energy. **87**(10), 3051–3064 (2010)
11. Aly, A. M.: Dynamic modeling and power management for stand-alone AC-coupled photovoltaic system. Energy Syst.1–19 (2015)
12. Pati, A. K., Sahoo, N. C.: A new approach in maximum power point tracking for a photovoltaic array with power management system using Fibonacci search algorithm under partial shading conditions. Energy Syst. **7**(1), 145–172 (2016)
13. Zelazo, D., Dai, R., Mesbahi, M.: An energy management system for off-grid power systems. Energy Syst. **3**(2), 153–179 (2012)
14. Morsli, S., Tayeb, A., Mouloud, D., Abdelkader, C.: A robust adaptive fuzzy control of a unified power flow controller. Turk. J. Electr. Eng. Comput. Sci. **20**(1), 87–98 (2012)
15. Kerekes, T., Séra, D., Máthé, L.: Three-phase Photovoltaic Systems: Structures, Topologies, and Control, Electr. Power Compon. Syst. **43**(12), 1364–1375 (2015)
16. Ibrahim H. E. A., Ibrahim, M.: Comparison Between Fuzzy and P&O Control for MPPT for Photovoltaic System Using Boost Converter. J. Energy Technol. Policy. **2**(6), 1–11 (2012)
17. Tourqui, D. E., Smaili, A., Betka, A., Allaoui, T., Denai, M.: Design and implementation of a digital MPPT controller for a photovoltaic panel.
18. Mary, S. S., Kumar, S. S., Poluru, S. P., Reddy, M. J. B.: A Dual DC Output Power Supply for a Stand-alone Photovoltaic System. Electr. Power Compon. Syst. **43**(8–10), 939–950 (2015)
19. Mei, Q., Shan, M., Liu, L., Guerrero, J. M.: A Novel Improved Variable Step-Size Incremental-Resistance MPPT Method for PV Systems. Ind. Electron. IEEE Trans. **58**(6), 2427–2434 (2011)
20. Liu, F., Duan, S. Liu, F., Liu, B., Kang, Y.: A Variable Step Size INC MPPT Method for PV Systems. Ind. Electron. IEEE Trans. **55**(7), 2622–2628 (2008)
21. Rezvani, A., Izadbakhsh, M., Gandomkar, M.: Enhancement of microgrid dynamic responses under fault conditions using artificial neural network for fast changes of photovoltaic radiation and FLC for wind turbine. Energy Syst. **6**(4), 551–584 (2015)
22. Alata, M., Al-Nimr, M. A., Qaroush, Y.: Developing a multipurpose sun tracking system using fuzzy control. Energy Convers. Manag. **46**(7–8), 1229–1245 (2005)
23. Ouada, M., Meridjet, M. S., Talbi, N.: Optimization photovoltaic pumping system based BLDC using fuzzy logic MPPT control. Renewable and Sustainable Energy Conference (IRSEC). 27–31 (2013)
24. Letting, L. K., Munda, J. L., Hamam, Y.: Optimization of a fuzzy logic controller for PV grid inverter control using S-function based PSO. Sol. Energy. **86**(6), 1689–1700 (2012)
25. Altin, N., Ozdemir, S.: Three-phase three-level grid interactive inverter with fuzzy logic based maximum power point tracking controller. Energy Convers. Manag. **69**,17–26 (2013)
26. Al Nabulsi, A., Dhaouadi, R.: Efficiency Optimization of a DSP-Based Standalone PV System Using Fuzzy Logic and Dual-MPPT Control. Ind. Inform. IEEE Trans. **8**(3), 573–584 (2012)

27. Rahmani, R., Seyedmahmoudian, M., Mekhilef, S., Yusof, R.: Implementation Of Fuzzy Logic Maximum Power Point Tracking Controller For Photovoltaic System. Am. J. Appl. Sci. **10**(3), 209 (2013)
28. Beltran, H., Swierczynski, M., Luna, A., Vazquez, G., Belenguer, E.: Photovoltaic plants generation improvement using Li-ion batteries as energy buffer. IEEE International Symposium on Industrial Electronics (ISIE), 2063–2069 (2011)
29. Naderi, P., Fallahi, F.: A novel structure proposal for distributed generation using SMES and PV system with relative controllers design. Energy Syst. **6**(2), 153–172 (2015)
30. Nair, N.-K. C., Garimella, N.: Battery energy storage systems: Assessment for small-scale renewable energy integration. Energy Build. **42**(11), 2124–2130 (2010)
31. Rejovitzky, E., Di Leo, C. V., Anand, L.: A theory and a simulation capability for the growth of a solid electrolyte interphase layer at an anode particle in a Li-ion. J. Mech. Phys. Solids. **78**, 210–230 (2015)
32. Salvadori, A., Grazioli, D., Geers, M. G. D.: Governing equations for a two-scale analysis of Li-ion battery cells. Int. J. Solids Struct. **59**. 90–109 (2015)
33. Yau, H.-T., Liang, Q.-C.; Hsieh, C.-T.: Maximum power point tracking and optimal Li-ion battery charging control for photovoltaic charging system. Comput. Math. Appl. **64**(5), 822–832 (2012)
34. Riffonneau, Y., Bacha, S., Barruel, F., Ploix, S., Optimal Power Flow Management for Grid Connected PV Systems With Batteries. Sustain. Energy IEEE Trans. **2**(3), 309–320 (2011)
35. Xiong, P., Peng, L., Chen, D., Zhao, Y., Wang, X., Yu, G.: Two-dimensional nanosheets based Li-ion full batteries with high rate capability and flexibility. Nano Energy. **12**. 816–823 (2015)
36. Eghtedarpour, N., Farjah, E.: Distributed charge/discharge control of energy storages in a renewable-energy-based DC micro-grid. Renew. Power Gener. IET. **8**(1). 45–57 (2014)
37. Aldaoudeyeh, A.-M. I.: Photovoltaic-battery scheme to enhance PV array characteristics in partial shading conditions. IET Renew. Power Gener. (2015)
38. Ahmad Hamidi, S., Ionel, D. M., Nasiri, A. Modeling and Management of Batteries and Ultracapacitors for Renewable Energy Support in Electric Power Systems–An Overview. Electr. Power Compon. Syst. **43**(12), 1434–1452 (2015)
39. Beltran, H., Swierczynski, M., Luna, A., Vazquez, G., Belenguer, E.: Photovoltaic plants generation improvement using Li-ion batteries as energy buffer. Industrial Electronics (ISIE), IEEE International Symposium. 2063–2069 (2011)
40. Wu, H., Wang, S., Zhao, B., Zhu, C.: Energy management and control strategy of a grid-connected PV/battery system. Int. Trans. Electr. Energy Syst. (2014)
41. Dearborn, S.: Charging Li-ion Batteries for Maximum Run Times. Power Electron Technol Mag. **31**(4), 40–49 (2005)
42. Eghtedarpour N., Farjah, E.: Control strategy for distributed integration of photovoltaic and energy storage systems in DC micro-grids. Renew. Energy. **45**. 96–110 (2012)
43. Kusakana K., Vermaak, H. J.: Hybrid diesel generator/renewable energy system performance modeling. Renew. Energy. **67**, 97–102 (2014)
44. Elmitwally, A., Rashed, M., Flexible Operation Strategy for an Isolated PV-Diesel Microgrid Without Energy Storage. Energy Convers. IEEE Trans. **26**(1), 235–244 (2011).
45. Luna, A., Blaabjerg, F., Rodríguez, P.: Control of Power Converters in AC Microgrids », Power Electron. IEEE Trans. **27**(11), 4734–4749 (2012)
46. Velasco de la Fuente, D., Rodríguez, C. L. T., Garcerá, G., Figueres, E., Gonzalez, R. O.: Photovoltaic Power System With Battery Backup With Grid-Connection and Islanded Operation Capabilities. Ind. Electron. IEEE Trans. **60**(4), 1571–1581 (2013)
47. Guerrero, J. M., Vasquez, J. C., Matas, J., Vicuna, D., García, L., Castilla, M.: Hierarchical Control of Droop-Controlled AC and DC Microgrids—A General Approach Toward Standardization. Ind. Electron. IEEE Trans. **58**(1), 158–172 (2011)
48. Kwon, J., Yoon, S., Choi, S.: Indirect Current Control for Seamless Transfer of Three-Phase Utility Interactive Inverters. Power Electron. IEEE Trans. **27**(2), 773–781 (2012)